Study of Pulsatile Non-Newtonian Blood Flow Through Abdominal Aorta and Renal Arteries Incorporating Fluid-Structure Interaction

Mortazavinia Z.[1], Goshtasbi Rad E.[2], Emdad H.[3], Sharifkazemi M. B.[4], Zare A.[5], Mehdizadeh A. R.*[6]

Abstract

Background: The interaction between the blood and the vessel wall is of great clinical interest in studying cardiovascular diseases, the major causes of death in developed countries.

Objective: To understand the effects of incorporating fluid-structure interaction into the simulation of blood flow through an anatomically realistic model of abdominal aorta and renal arteries reconstructed from CT images.

Methods: The fluid is assumed to be incompressible and non-Newtonian and the vessel wall is set to have isotropic elastic properties. The blood flow is assumed to be periodic; therefore, a real pulsatile flow velocity in the entrance of the abdominal aorta of a healthy adult is measured via laser Doppler anemometry and used in this study. The effects of wall flexibility, both rigid and compliant models were also simulated.

Results: Comparison of the rigid model with compliant model reveals that velocity and pressure drop in flexible arteries is less than those in rigid arteries. As wall shear stress plays an important role in the function of the cardiovascular system as it has immediate effect on the endothelial histology, the wall shear stress was analyzed; the rigid model wall shear stress magnitude was higher than that in the compliant model. It was also observed that the peak values of wall shear stress in this study were not high enough to be able to damage and strip the endothelial cells. Displacements of vessel walls were also studied; it was found that the wall displacement during the systole was higher than the diastole.

Conclusion: Incorporating fluid-structure interaction and considering vessel wall deformations in studying blood flow through arteries have notable effects on blood flow characteristics.

Keywords

Blood flow, pulsatile; Abdominal aorta; Renal arteries

[1]Department of Mechanical Engineering, ÉcolePolytechnique de Montréal, Montreal, Canada
[2]School of Mechanical Engineering, Shiraz University, Shiraz, Iran
[3]School of Mechanical Engineering, Shiraz University, Shiraz, Iran
[4]Shiraz Medical School, Shiraz University of Medical Science, Shiraz, Iran
[5]Department of Mechanical Engineering, Islamic Azad University, Shiraz Branch, Member of Young Researchers Club, Shiraz, Iran
[6]Center for Research in Medical Physics and Engineering, School of Medicine, Shiraz University of Medical Science, Shiraz, Iran

*Corresponding author: Alireza Mehdizadeh, MD, PhD, Assistant Professor of Medical Physics, Room No. 702, Department of Medical Physics, School of Medicine, Shiraz University of Medical Science, Shiraz, Iran
E-mail: mehdizade@sums.ac.ir
Tel/Fax: +98-711-234-9332

Introduction

The interaction between the blood and the vessel wall is of great clinical interest in studying cardiovascular diseases, the major causes of death in developed countries [1]. In recent years, computational mechanics has made notable progress in simulation of accurate blood flow in realistic anatomical models constructed from 3D medical imaging data. Simulations of blood flow through aorta have been mostly limited to a single branch [2-4]. Actually, most of the arter-

ies are multi-branched; therefore, it is believed that the flow fields among branches are complicated. Later, the steady blood flow in two vertical branches [5] and their four branches, *i.e.*, renal and iliac arteries [6], were studied. Accurate blood flows in more complete models were studied experimentally [7-12]. Numerically, Taylor, *et al*. [13, 14], employed a finite element method and simulated the 3D blood flow in the abdominal aorta. Kim, *et al*. [15], considered the interactions between heart and the arterial system and obtained physiologically realistic aortic flow and pressure waveforms for both the rest and exercise conditions. Blood flow in the systemic arteries such as renal, carotid, subclavian, brachial, iliac, and the femoral arteries was studied by Olufsen, *et al*. [16], assuming different conditions for large and small arteries.

Researchers have shown that the time-varying nature of blood flow within the arteries cannot be neglected in realistic conditions. Other studies have thus, included transient conditions into their simulations to take into account this flow behavior [13, 14, 17, 18].

Assuming a Newtonian behavior for blood is only acceptable when it has shear rates more than 100 s^{-1}, which commonly occurs in large arteries [19, 20]. In most cases, though, non-Newtonian models provide a more realistic representation of blood flow behavior [21, 22]. Several non-Newtonian models have been proposed to explain the stress-strain relationship for blood [23, 24]. However, none of these models reflects the true behavior of the blood rheology. The Carreau non-Newtonian model, as used by Cho and Kensey [24] and Johnston, *et al*. [21], has been found to fit the blood flow experimental data quite well and not over-predict the non-Newtonian effects.

Computer-based simulation tools are getting integrated to solve interactions between different disciplines such as fluid-structure interaction (FSI). One of the FSI applications is in blood flow through flexible arteries. Lee and Xu simulated transient blood flow within a compliant vessel [25]. They continued the earlier experiment by Ohja, *et al*. [26] and used an isotropic elastic solid, close to artery conditions, to represent the vessel walls. They concluded that expansion of the arteries due to internal blood pressure causes slower fluid flow. They also observed the time-dependent fluid velocity and structural displacements. Chan, *et al*., [27] continued Lee and Xu's study [25], but investigated power law and Carreau non-Newtonian models to represent the blood flow.

The objective of the present study was to simulate a pulsatile blood flow through an anatomically realistic model of abdominal aorta and renal arteries which was reconstructed from CT images, considering vessel wall flexibility. To investigate the reciprocal effects of internal blood flow and vessel walls, the finite element and finite volume-based commercial codes ANSYS Workbench and CFX were used, respectively. Incorporating FSI, the effects of vessel wall deformation on parameters such as flow velocity, pressure and wall shear stress were also investigated. To validate the numerical methods employed in this study, we also compared our findings with the study of Chan *et al*. [27].

Materials and Methods

FSI occurs whenever the problem involves the flow of a fluid causing deformation of a solid structure. This deformation, in turn, changes the boundary conditions of the fluid field. In the present study, an iterative two-way coupling method was used to link the fluid and solid portions. To achieve this, ANSYS software package consisting of programs ANSYS Workbench and CFX was used; they are capable of modeling the structural and fluid domains, respectively.

Governing equations

The blood flow in vessels is commonly laminar. This is the normal condition for blood flow throughout most parts of the circulatory system [28]. For unsteady laminar flow of

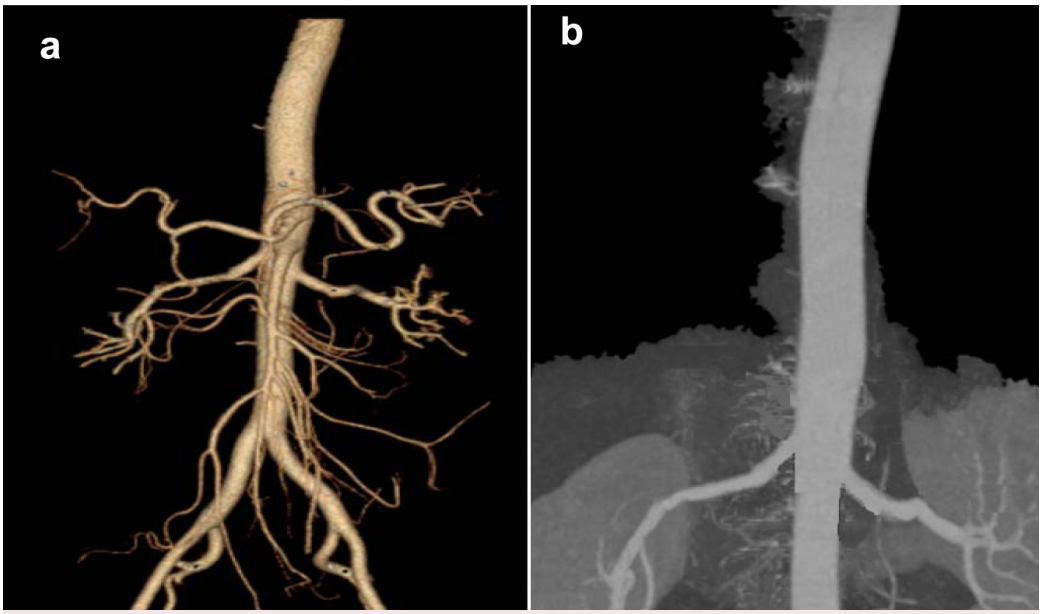

Figure 1: CT images of abdominal aorta and a) arterial branches b) renal arteries

an incompressible, non-Newtonian fluid, the mass and momentum equations (ignoring the body forces) can be written as [29]:

$$\frac{\partial U_i}{\partial x_i} = 0 \qquad (1)$$

$$\frac{\partial U_i}{\partial t} + \frac{\partial (U_i U_j)}{\partial x_j} = \frac{1}{\rho_f}\left[-\frac{\partial p}{\partial x_i} + \frac{\partial}{\partial x_j}\left(\mu \left(\frac{\partial U_i}{\partial x_j} + \frac{\partial U_j}{\partial x_i} \right) \right) \right] \qquad (2)$$

where U_i denotes velocity components; and ρ and μ are fluid density and viscosity, respectively; p is the pressure.

For the vessel wall, which is defined as an elastic solid, the relationship between stress and displacement (ignoring body forces) can be expressed as [29]:

$$\rho_w \frac{\partial^2 d_i}{\partial t^2} = \frac{\partial \sigma_{ij}}{\partial x_j} \qquad (3)$$

where d_i and σ_{ij} are the components of the displacements and stress tensor in solid, respectively, and ρ_w is the wall density.

σ_{ij} can be obtained from the constitutive equation of the material. For a Hookean elastic solid, it is [29]:

$$\sigma_{ij} = \lambda e_{kk} \delta_{ij} + 2\mu_L e_{ij} \qquad (4)$$

where λ and μ_L are the Lame's constants, δ_{ij} is the Kronecker delta and e_{ij} are the components of the strain tensor which can be expressed as [29]:

$$e_{ij} = \frac{1}{2}\left(\frac{\partial d_i}{\partial x_j} + \frac{\partial d_j}{\partial x_i} \right) \qquad (5)$$

Lame's constants are related to physical properties of material, Young's modulus, E, and Poisson's ratio, υ, by the following equations [29]:

$$\lambda = \frac{\upsilon E}{(1+\upsilon)(1-2\upsilon)} \qquad (6)$$

$$\mu_L = \frac{E}{2(1+\upsilon)} \qquad (7)$$

Geometry

An anatomically realistic model of abdominal aorta constructed from CT images is shown in Figure 1a. As discussed above, the main objective of this study was to simulate blood flow through abdominal aorta and renal arteries. Therefore, Figure 1b, which shows only abdominal aorta and renal arteries, was reconstructed out of Figure 1a.

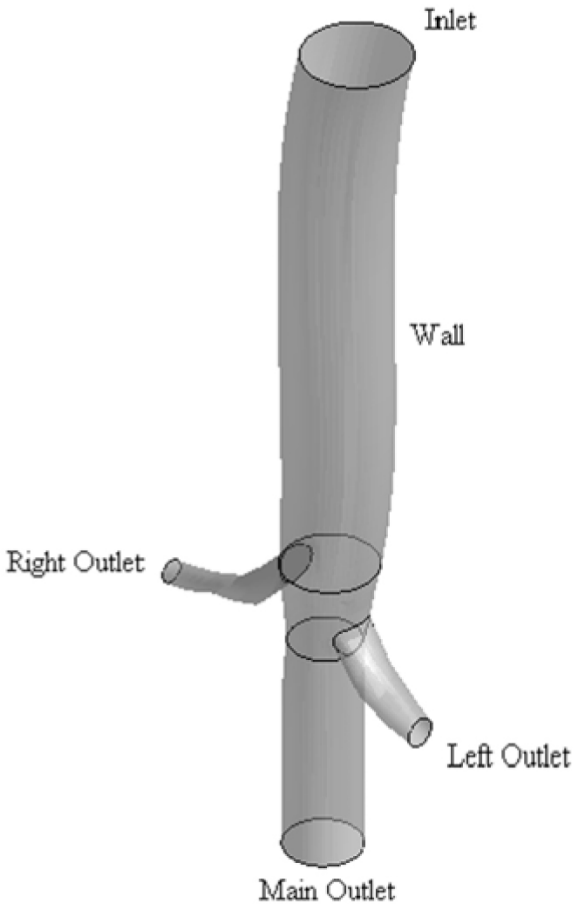

Figure 2: Basic model geometry, reconstructed from CT images

The simplified model (Fig. 2) is aorta and renal arteries reconstructed from Figure 1, using a computer aided design (CAD) software. The inlet and outlet diameters of the main aorta were 18 and 13 mm, respectively. Also, outlet diameters of left and right renal arteries were 5 and 4 mm, respectively. The wall thicknesses of the aorta and renal arteries were 2 and 1 mm, respectively [28].

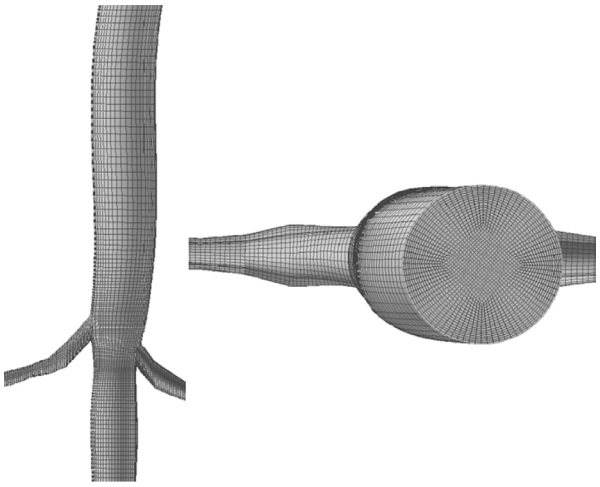

Figure 3: Structured mesh for computational domain

It is necessary to have a proper mesh technique to provide accurate answers while not exceeding computational power. Due to the geometry complexity, multi-block meshing technique was used to create structured mesh in computational domains and to prevent high grid concentration in the center of the circular cross sections (Fig. 3). The generated structured grid consists of 415,440 hexahedral elements, by performing grid study. Since the wall shear stress is sensible to mesh density, it was verified that the mesh used in the simulation provided a converged solution for the wall shear stress.

Material properties

In the present study, blood was assumed to have a density of 1050 kg/m^3. Carreau non-Newtonian model, which has been shown to fit the blood flow experimental data quite well and not over-predict the non-Newtonian effects [22, 24], was used to define the viscosity. In this model, the relation between viscosity and shear strain rate, $\dot{\gamma}$, can be written as [21]:

Where λ_f = 3.313 s; zero strain viscosity, μ_0 = 0.056 Pa.s; infinite strain viscosity, μ_∞ = 0.00345 Pa.s; and the empirical exponent, n =0.3568.

The vessel wall was considered to be linearly elastic, isotropic and nearly incompressible with a Young's modulus of 4.66 MPa, a Poisson's ratio of 0.45 and a density of 1062 kg/m^3 [30].

Boundary conditions

The blood flow was assumed to be periodic; therefore, a real pulsatile flow velocity at the entrance of abdominal aorta of a healthy adult was measured via laser Doppler anemometry (LDA) and used in this study. Figure 4 shows the waveform inlet velocity, u(t), with a time period (t_p) of 0.82 s.

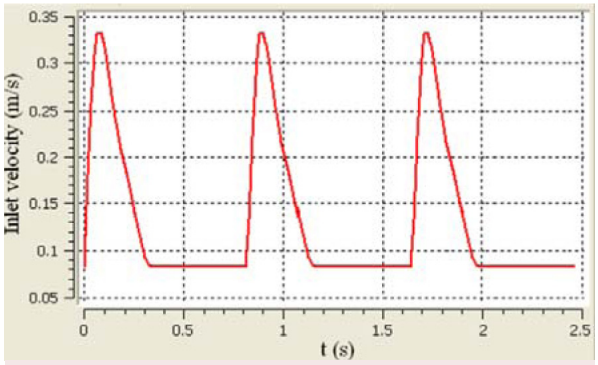

Figure 4: Time variation of the inlet velocity, $u(t)$

The mean arterial pressure (MAP) takes account of pulsatile blood flow in the arteries, and is the best measure of perfusion pressure to an organ [28]. For the main outlet boundary, a constant pressure of 11,500 Pa (the MAP through aorta) was assumed. A mean pressure of 11,000 and 11,200 Pa was assumed for the right and left renal arteries outlet pressure, respectively. An appropriate boundary condition was applied on walls to indicate the interfaces on which FSI occurred. This allowed the transfer of fluid forces and solid displacements across the specified boundaries. The solid model corresponding to the vessel wall was assumed to be fixed at the outlet of renal arteries, because of their connection to the kidneys. The inlet and outlet of aorta were exposed to a boundary condition, such that only movement in the radial-tangential plane was allowed.

Results and Discussion

Validation of FSI models

To validate the methods employed in this study, we compared our findings with the numerical study by Chan, *et al*. [27].. They studied pulsatile blood flow in a flexible stenosed artery (Fig. 5) and used a sinusoidal volumetric flow waveform of 4.3±2.6 mL/s at the inlet with a period of t_p of 0.345 s. A constant pressure of 4140 Pa was specified at the outlet.

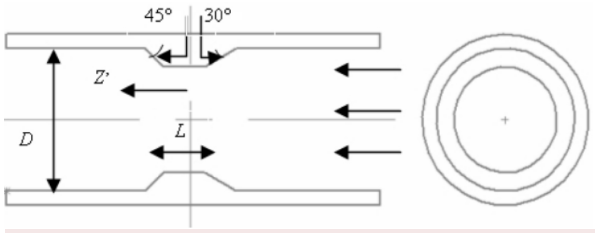

Figure 5: Stenosed artery uesd by Chan, *et al*. [27], L= 1.5 mm, D=5 mm, and $Z'=Z/D$ is the normalized distance from the center of stenosis.

The results for axial velocity profile and wall shear stress for Carreau non-Newtonian model are presented in Figures 6 and 7. The parameter t/t_p was used to describe a particular time in a cycle. The term t represents the time in seconds and t_p is the period of the flow cycle.

According to these figures, there is acceptable agreement between the results obtained by the two compared studies.

Basic model results

To study the effects of wall flexibility, both rigid and compliant models were simulated.

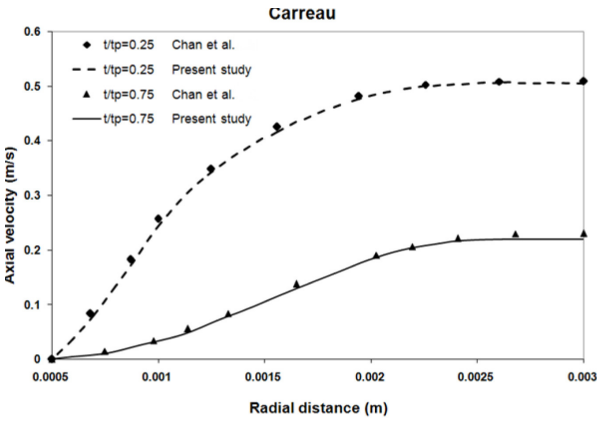

Figure 6: Axialvelocity profile at Z'=4.3

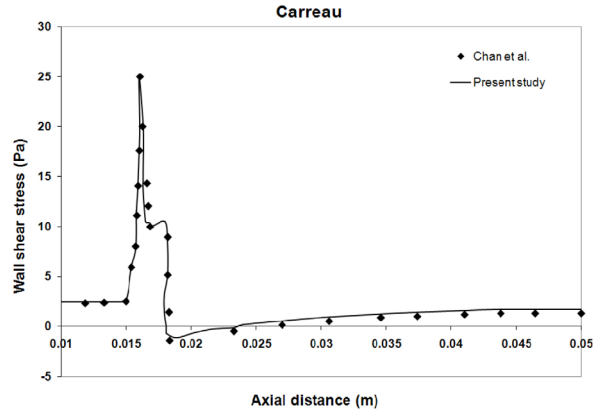

Figure 7: Wall shear stress along the axial distance at t/t_p= 0.25

Table 1: Selected time frames

t/t_p	Inlet velocity state
0.04	Midway-systolic
0.10	Maximum flow
0.37	Midway-diastolic
1.00	Minimum flow

Simulations were carried out over at least three complete cycles to achieve a periodic solution; the results were saved for the final cycle.

The selected times corresponding to the periodic inlet velocity presented in Figure 4, are shown in Table 1.

Velocity

Plots of velocity distribution in the region of interest, at selected time frames are shown in Figure 8 where both rigid and compliant models are presented for comparison. The figures indicate that the flow velocity in rigid wall model is higher than the compliant model. This can be explained by the mass conservation theory: the fluid internal pressure exerted on the vessel wall, which remains above zero even during deceleration phase, pushes the vessel wall outward consistently and slows the fluid flow due to the flow area expansion.

Wall shear stress

Wall shear stress plays an important role in the vessel wall behavior in the cases where structural response can be responsible for wall rupture. To investigate shear stress on renal arteries walls, four paths were defined on the upper and bottom wall of the renal arteries medi-

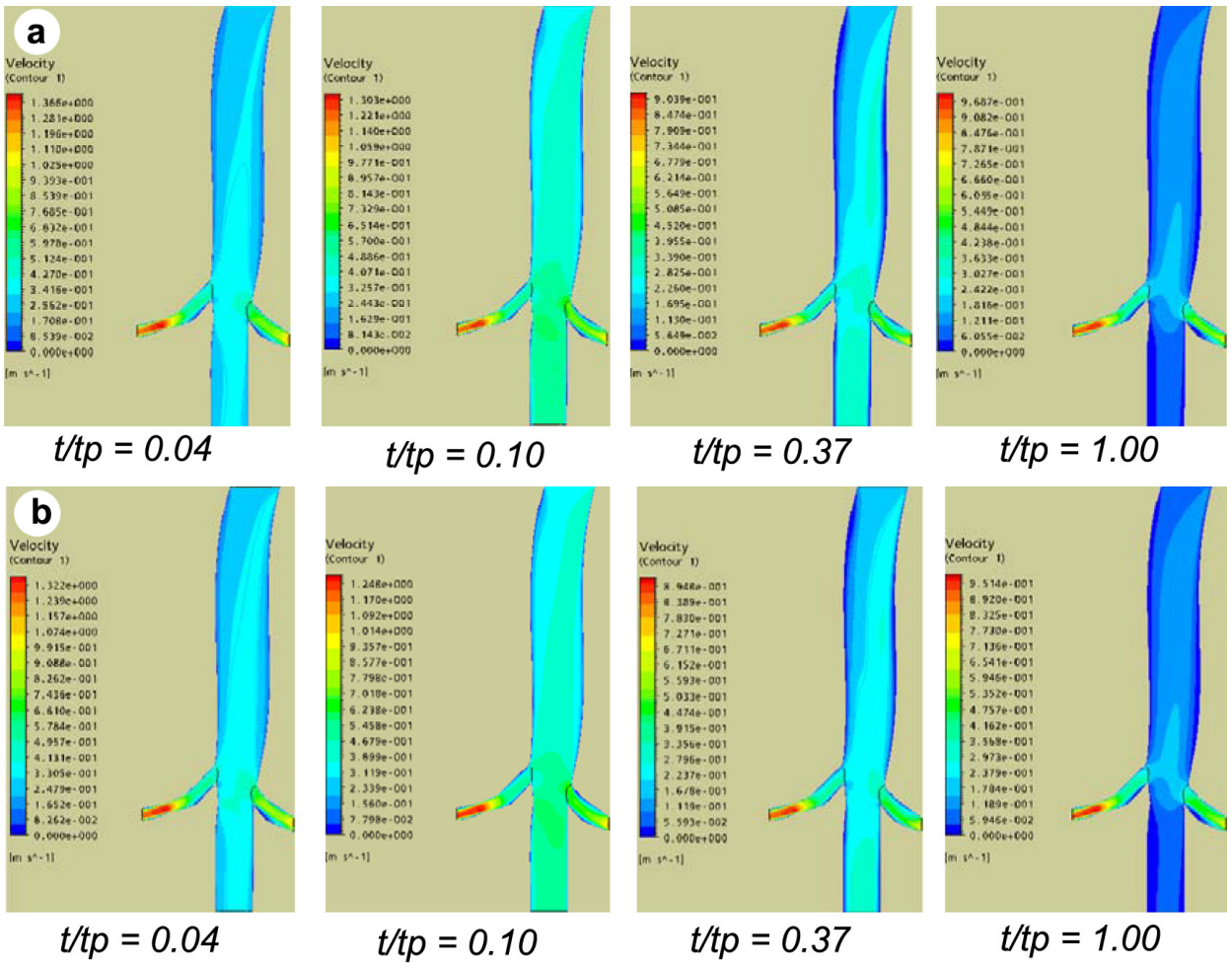

Figure 8: Plots of velocity distribution at selected time frames: (a) Rigid model (b) Compliant model

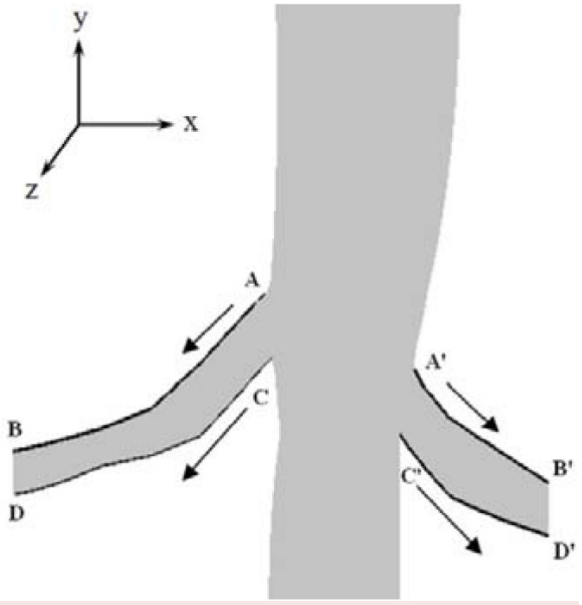

Figure 9: Defined paths and their corresponding directions on renal arteries walls, to study wall shear stress

al plane. These paths and their corresponding directions are shown in Figures 9. Figure 10 shows the wall shear stress variations in rigid and compliant models at peak flow time of t/t_p of 0.10 over the selected length of the walls.

It is obvious that wall shear stress is directly related to the rate of velocity change near the wall, which is caused by the change in geometry. In other words, any change of the geometry in artery produces significant effects on blood flow. The flow experiences high shear stresses as it is forced through the narrow passageway. It is also apparent in this figure that the magnitude in rigid model wall shear stress is higher than that in the FSI model—approximately 0.28 times the value at the highest peak in Figure 10 (along path A-B). This is mainly due to the fact that the velocity gradient near the wall decreases by considering FSI.

Fry [31] concluded that wall shear stress has immediate effect on the endothelial histology and a shear stress of 40 Pa is able to damage the endothelial cells. Another research conducted by Ramstack, *et al*. [32], showed that higher wall shear stress can strip the endothelial cells and prevent the endothelium from inhibiting thrombogenesis. This study showed

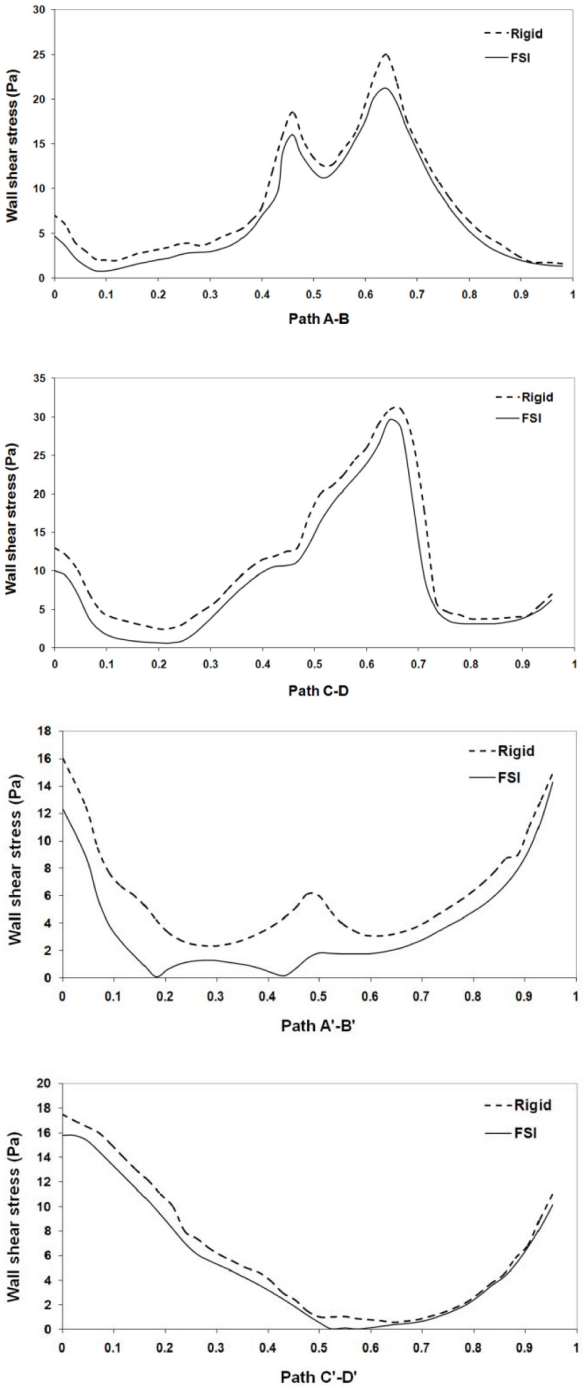

Figure 10: Wall shear stress distributions for the rigid and FSI models at peak flow time, t/t_p = 0.10, along the defined paths

that the peak wall shear stress did not reach 40 Pa in the arteries and therefore the endothelial cells would neither damaged nor stripped.

Displacement

The total displacement of the vessel wall

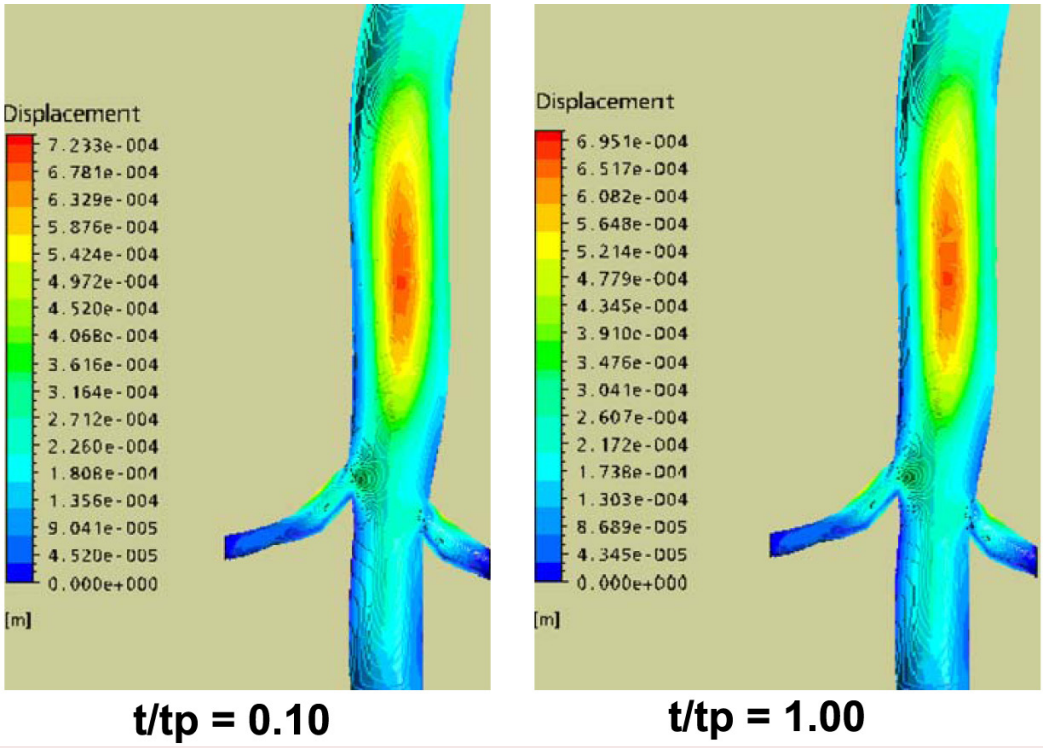

Figure 11: Contours of wall displacements at two selected times

is depicted in Figure 11 at two selected time points of the wave, *i.e.*, t/t_p = 0.10, and t/t_p = 1.00 corresponding to the maximum and minimum flow, respectively. It is seen that renal arteries and their corresponding end supports, kidneys, cause the aorta not to deform uniformly in X-Z plane. Therefore, aorta wall deformation in Z-direction is more than other directions. The time-dependent deformation is a result of the fluid pulsatile pressure loading via the FSI coupling. It was found that wall displacement during the systole, in which the flow is accelerating, was higher than the diastole.

Conclusion

The objective of this study was to provide an understanding of the effects of incorporating FSI into the simulation of a pulsatile non-Newtonian blood flow through an anatomically realistic model of abdominal aorta and renal arteries reconstructed from CT images. We found that the fluid pressure exerted on the inner wall of the vessels, even during the deceleration phase of diastole, consistently pushes the wall outward expanding the flow area. This wall expansion causes the flow velocity in the rigid wall model to be higher than the compliant model.

Comparison between the rigid and compliant models revealed that by incorporating FSI analysis, the flow pressure drops and the wall shear stress decreases. This is mainly due to the fact that the wall shear stress is directly related to the rate of velocity change near the wall, which decreases by considering FSI.

Furthermore, it was concluded that the wall deformability has almost no significant effect on pressure and velocity values through arteries; although it has notable effect on the wall shear stress, which is of great clinical interest. Rigid wall simulation of blood flow through arteries over-predicts the wall shear stress. It was also observed that the peak values of the wall shear stress in this study were not high enough to be able to damage or strip the endothelial cells.

The time-dependent deformation of the ves-

sel walls is a result of fluid pulsatile pressure loading via the FSI coupling. It was found that the wall displacement during the systole was higher than the diastole.

These findings showed that incorporating FSI and considering vessel wall deformations in studying blood flow through arteries have significant effects on blood flow characteristics.

References

1. Ku DN. Blood flow in arteries. *Annu Rev Fluid Mech* 1997;**29**:399-434.
2. Perktold K, Peter R, Resch M. Pulsatile non-Newtonian blood flow simulation through a bifurcation with an aneurysm. *J Biorheol* 1989;**26**:1011-30.
3. Rindt CCM, Van Steenhoven AA. Unsteady flow in a rigid three-dimensional model of the carotid artery bifurcation. *J Biomech* 1996;**118**:90-6.
4. Lee D, Chiu YL, Jen CY. Wall stresses and platelet adhesion in a T-junction. *Proc Natl Sci Counc ROC(A)* 1999;**23**:303-10.
5. Lee D, Chen JY. Numerical simulation of flow fields in a tube with two branches. *J Biomech* 2000;**33**:1305-12.
6. Shipkowitz T, Rodgers VGJ, Frazin LJ, Chandran KB. Numerical study on the effect of secondary flow in the human aorta on local shear stresses in abdominal aortic branches. *J Biomech* 2000; **33**:717-28.
7. Liepsch D, Poll A, Strigberger J, *et al.* Flow visualization studies in a mold of the normal human aorta and renal arteries. *J Biomech Eng* 1989;**111**:222-7.
8. Moore Jr, JE, Ku DN, *et al.* Pulsatile flow visualization in the abdominal aorta under differing physiologic conditions: implications for increased susceptibility. *J Biomech Eng* 1992; **114**:391-7.
9. Moore Jr, JE, Ku DN. Pulsatile velocity measurements in a model of the human abdominal aorta under resting conditions. *J Biomech Eng* 1994; **116**:337-46.
10. Moore Jr, JE, Ku DN. Pulsatile velocity measurements in a model of the human abdominal aorta under simulated exercise and postprandial conditions. J Biomech Eng 1994;**116**:107-11.
11. Pedersen EM, Sung HW, Yoganathan AP. Influence of abdominal aortic curvature and resting versus exercise conditions on velocity fields in the normal abdominal aortic bifurcation. *J Biomech Eng* 1994;**116**:347-54.
12. Barakat AI, Karino T, Colton C. Microcinematographic studies of flow patterns in the excised rabbit aorta and its major branches. *J Biorheol* 1997;**34**:199-221.
13. Taylor CA, Hughes TJR, Zarins CK. Finite element modeling of three-dimensional pulsatile flow in the abdominal aorta: relevance to atherosclerosis. *Ann Biomed Eng* 1998;**26**:975-87.
14. Taylor CA, Hughes TJR, Zarins CK. Effect of exercise on hemodynamic conditions in the abdominal aorta. *J Vasc Surg* 1999;**29**:1077-89.
15. Kim HJ, Vignon-Clementel IE, Figueroa CA, *et al.* On coupling a lumped parameter heart model and a three dimensional finite element aorta model. *Ann Biomed Eng* 2009;**37**:2153-69.
16. Olufsen MS, Peskin CS, Kim WY, *et al.* Numerical Simulation and Experimental Validation of Blood Flow in Arteries with Structured-Tree Outflow Conditions. *Ann Biomed Eng* 2000;**28**:1281-99.
17. Grinberg L, Cheever E, Anor T, *et al.* Modeling blood flow circulation in intracranial arterial networks: A comparative 3D/1D simulation study. *Ann Biomed Eng* 2010; DOI: 10.1007/s10439-010-0132-1.
18. Tu C, Deville M. Pulsatile flow of non-Newtonian fluids through arterial stenoses. *J Biomech* 1996; **29**:899-908.
19. Pedley TJ. *The Fluid Mechanics of Large Blood Vessels*. Cambridge: Cambridge Univ Press; *1980*.
20. Berger SA, Jou L-D. Flow in stenotic vessels. *Annu Rev Fluid Mech* 2000;**32**:347-82.
21. Johnston BM, Johnston PR, Corney S, Kilpatrick D. Non-Newtonian blood flow in human right coronary arteries: steady state simulations. *J Biomech* 2004;**37**:709-20.
22. Johnston BM, Johnston PR, Corney S, Kilpatrick D. Non-Newtonian blood flow in human right coronary arteries: Transient simulations. *J Biomech* 2006;**39**:1116-28.
23. Walburn FJ, Schneck DJ. A constitutive equation for whole human blood. *J Biorheol* 1976;**13**:201-10.
24. Cho YI, Kensey KR. Effects of the non-Newtonian viscosity of blood in flows in a diseased arterial vessel. Part 1: Steady flows. *J Biorheol* 1991;**28**:241-62.
25. Ballyk PD, Steinman DA, Etheir CR. Simulation of non-Newtonian blood flow in an end-to-side anastomosis. *J Biorheol* 1994;**31**:565-86.
26. Lee KW, Xu XY. Modeling of flow and wall behaviour in a mildly stenosed tube. *J Med Eng Phys* 2002;**24**:575-86.

27. Ohja M, Cobbold RSC, Johnston KW, Hummel RL. Pulsatile flow through constricted tubes: an experimental investigation using photochromic tracer methods. *J Fluid Mech* 1989;**203**:173-97.
28. Chan W, Ding Y, Tu JY. Modeling of non-Newtonian blood flow through a stenosed artery incorporating fluid-structure interaction. *ANZIAM J* 2007;**47**:507-23.
29. Ganong WF. *Review of medical physiology*. California: Appleton & Lange;**1988**.
30. Lai WM, Rubin D, Krempl E. *Introduction to Continuum Mechanics*. Burlington: Elsevier Science; **1999**.
31. Giannakoulas G, Giannoglou G, Soulis J, *et al*. A computational model to predict aortic wall stresses in patients with systolic arterial hypertension. *Med Hypotheses* 2005;**65**:1191-5.
32. Fry DL. Acute vascular endothelial changes associated with increased blood velocity gradients. *Circ Res* 1968;**22**:165-97.
33. Ramstack JM, Zuckerman L, Mockros LF. Shear induced activation of platelets. *J Biomech* 1979;**12**:113-25.